

# An Automatic Beat Detection Algorithm for Pressure Signals

Mateo Aboy\*, *Member, IEEE*, James McNames, *Senior Member, IEEE*, Tran Thong, *Fellow, IEEE*, Daniel Tsunami, Miles S. Ellenby, and Brahm Goldstein, *Associate Member, IEEE*

**Abstract**—Beat detection algorithms have many clinical applications including pulse oximetry, cardiac arrhythmia detection, and cardiac output monitoring. Most of these algorithms have been developed by medical device companies and are proprietary. Thus, researchers who wish to investigate pulse contour analysis must rely on manual annotations or develop their own algorithms. We designed an automatic detection algorithm for pressure signals that locates the first peak following each heart beat. This is called the percussion peak in intracranial pressure (ICP) signals and the systolic peak in arterial blood pressure (ABP) and pulse oximetry ( $\text{SpO}_2$ ) signals. The algorithm incorporates a filter bank with variable cutoff frequencies, spectral estimates of the heart rate, rank-order nonlinear filters, and decision logic. We prospectively measured the performance of the algorithm compared to expert annotations of ICP, ABP, and  $\text{SpO}_2$  signals acquired from pediatric intensive care unit patients. The algorithm achieved a sensitivity of 99.36% and positive predictivity of 98.43% on a dataset consisting of 42,539 beats.

**Index Terms**—Arterial blood pressure (ABP), component detection, intracranial pressure (ICP), pressure beat detection, pulse contour analysis, pulse oximetry ( $\text{SpO}_2$ ).

## I. INTRODUCTION

**A**UTOMATIC beat detection algorithms are essential for many types of biomedical signal analysis and patient monitoring. This type of analysis is most often applied to the electrocardiogram (ECG) signal in which one or more of its components is detected automatically. Although many detection algorithms have been developed for ECG signals [1], there are only a few publications that describe algorithms to detect features in pressure signals [2]–[5]. Since pressure detection algorithms are necessary for most types of pulse oximeters and devices that monitor cardiac output, most of these algorithms have been developed by medical device companies

Manuscript received October 30, 2003; revised November 14, 2004. This work was supported in part by the Thrasher Research Foundation, in part by the Northwest Health Foundation, and in part by the Doernbecher Children's Hospital Foundation. *Asterisk indicates corresponding author.*

\*M. Aboy is with the Electronics Engineering Technology Department, Oregon Institute of Technology, Portland, OR 97229 USA and also with the Biomedical Signal Processing Laboratory, Department of Electrical and Computer Engineering at Portland State University, 1900 SW 4th Ave., Portland, OR 97201 USA (e-mail: mateoaboy@ieee.org).

J. McNames and D. Tsunami are with the Biomedical Signal Processing Laboratory, Department of Electrical and Computer Engineering at Portland State University, Portland, OR 97201 USA.

T. Thong is with the Department of Biomedical Engineering, OGI School of Science and Engineering, Oregon Health and Science University, Portland, OR 97201 USA.

M. S. Ellenby and B. Goldstein are with the Complex Systems Laboratory in the Department of Pediatrics, Oregon Health and Science University, Portland, OR 97201 USA.

Digital Object Identifier 10.1109/TBME.2005.855725

and are proprietary. This forces researchers to either manually annotate short segments or implement their own semi-automatic algorithms that lack the performance, generality, and robustness of modern detection algorithms for ECG signals [6]. Most of these semi-automatic algorithms for pressure signals have not been rigorously validated or published.

We describe an automatic detection algorithm that identifies the time-location of the percussion component in intracranial pressure (ICP) and the systolic peak in ABP and  $\text{SpO}_2$  signals. The algorithm is designed for subjects without significant cardiac dysrhythmias. In Sections I–A–I–D, we describe the clinical relevance of pressure beat detection algorithms, give an overview of detection algorithms and describe the beat components common to pressure signals. Section II describes the detection algorithm in detail, including pseudocode to implement the different modules. Section III describes the validation database, benchmark parameters, and the performance criteria. Section IV reports the results of the performance assessment, and Section V discusses the algorithm's performance, limitations, and computational efficiency.

### A. Clinical Significance

The unavailability of robust detection algorithms for pressure signals has, at least partially, prevented researchers from fully conducting beat-by-beat analysis. Current methods of ICP signal analysis are primarily based on time- or frequency-domain metrics such as mean, standard deviation, and spectral power at the heart rate frequency [7]. Few investigators have analyzed variations in the beat-level morphology of the pressure signals because detection algorithms that can automatically identify each of the beat components are generally unavailable.

Many researchers manually annotate desired components of physiologic pressure signals because detection algorithms for these signals are not widely available. This approach is labor-intensive, subjective, expensive, and can only be used on short signal segments.

There are numerous current and potential applications for pressure beat detection algorithms. Many pulse oximeters perform beat detection as part of the signal processing necessary to estimate oxygen saturation, but these algorithms are proprietary and cannot be used in other applications. Systolic peak detection is necessary for some measures of baroreflex sensitivity [8]–[10]. Identification of the pressure components is necessary for some methods that assess the interaction between respiration and beat-by-beat ventricular parameters and the modulation effects of respiration on left ventricular size and stroke volume [11]. Detection is a necessary task when analyzing arterial compliance and the pressure pulse contour [12]. Beat-to-beat morphology analysis of ICP also requires robust automatic detection.

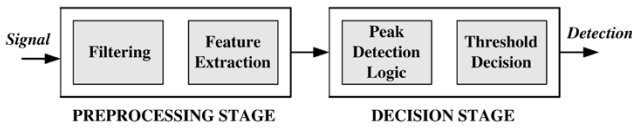


Fig. 1. Common architecture of detection algorithms. A preprocessing stage emphasizes the desired components and a decision stage performs the actual component detection.

### B. Overview of Beat Detection Algorithms

Most physiologic signal detection algorithms can be divided into two stages. As shown in Fig. 1, a preprocessing stage emphasizes the desired components in order to maximize the signal-to-noise ratio (SNR) and a decision stage decides if an incoming peak is a true component based on a user-specified threshold. This architecture has been employed in most ECG detection algorithms. The preprocessing stage traditionally relies on signal derivatives and digital filters [13]–[21]. Recent algorithms use wavelets and filter banks for preprocessing [22], [23].

### C. Pressure Pulse Morphology

The pulse morphology of ABP and  $\text{SpO}_2$  signals is well known and consists of a systolic peak, dichrotic notch, and dichrotic peak [24]. ICP has a similar pulse morphology, but often has a third peak. The three peaks common to ICP signals are the percussion ( $P_1$ ), tidal ( $P_2$ ), and dichrotic ( $P_3$ ) peaks. In this paper, we refer to the percussion (ICP) and systolic (ABP and  $\text{SpO}_2$ ) peaks as  $P_1$ . The valley between  $P_2$  and  $P_3$  in ICP signals is termed the dichrotic notch, and corresponds to the dichrotic notch in arterial blood pressure. The  $P_1$  component is a sharp peak, with fairly constant amplitude. In low-pressure ICP signals, the  $P_1$  component has the highest amplitude. The  $P_2$  component is more variable and is not always present in low-pressure ICP signals. Fig. 2 shows an example of a low-pressure ICP signal and its components. In high-pressure ICP signals, the  $P_2$  component is always present and usually has the highest amplitude. Fig. 3 shows an example of a high-pressure ICP signal. The physiology underlying the ICP pulse morphology and its components is reviewed in [25].

### D. Differences Between ECG and Pressure Signals

Pressure signals have a different time-domain morphology and spectral density than ECG signals. Since most of the ECG signal power is in the 10–25 Hz range, almost all QRS detection algorithms use a bandpass filter with these cutoff frequencies in the preprocessing stage to reduce out-of-band noise. These algorithms combine the filter operation with another transformation, such as the signal derivative or the dyadic wavelet transform, to exploit the large slope and high frequency content of the QRS complex. This transformation generates a feature signal in which QRS complexes can be detected by a simple threshold.

Since pressure signals are more sinusoidal and less impulsive than ECG signals, most of the signal power is in a lower frequency range that includes the fundamental frequency, typically from 0.7–3.5 Hz in humans. Thus, preprocessing and decision logic that rely on the impulsive shape of the QRS complex to improve detection accuracy are inappropriate for pressure signals and can reduce accuracy.

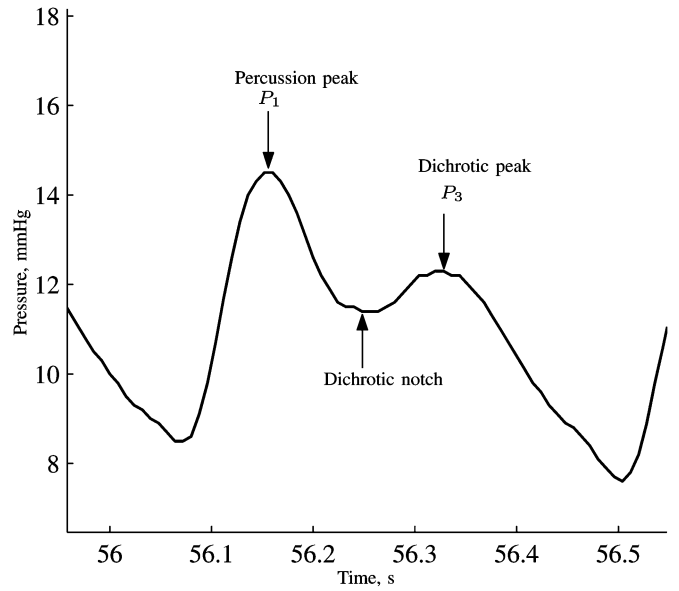


Fig. 2. Example of an ICP pulse showing the percussion peak ( $P_1$ ), dichrotic peak ( $P_3$ ), and dichrotic notch in a low-pressure ICP signal. Note that the tidal peak ( $P_2$ ) is absent in this case, and the ( $P_1$ ) component has the highest amplitude.

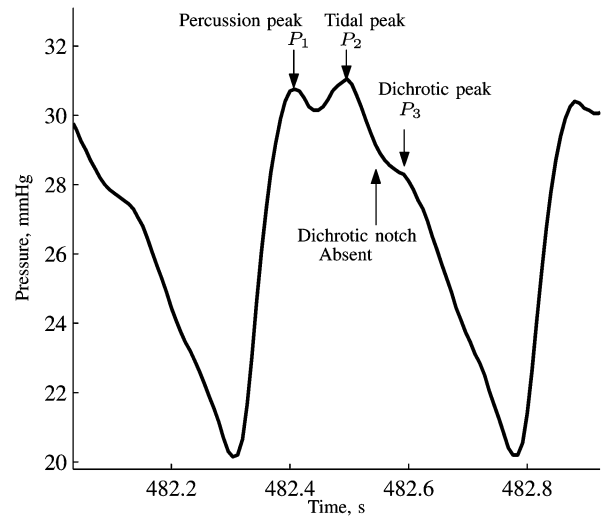


Fig. 3. Example of an ICP pulse showing the percussion peak ( $P_1$ ), tidal peak ( $P_2$ ), and dichrotic peak ( $P_3$ ) in a high-pressure ICP signal. Note that the tidal peak ( $P_2$ ) has the highest amplitude in this case, and the dichrotic notch is absent. These are characteristic features of a high-pressure ICP pulse morphology.

## II. ALGORITHM DESCRIPTION & THEORY

### A. Algorithm Overview

Fig. 4 shows a block diagram of our detection algorithm. The pressure signal is preprocessed by three bandpass elliptic filters with different cutoff frequencies. The output of the first bandpass filter is used to estimate the heart rate based on the estimated power spectral density (PSD). The estimated heart rate is then used to calculate the cutoff frequencies of the other two filters. Peak detection and decision logic are based on rank-order (percentile-based) nonlinear filters, that incorporate relative amplitude and slope information to coarsely estimate the percussion and systolic peak components ( $P_1$ ). A nearest neighbor algorithm combines information extracted from the

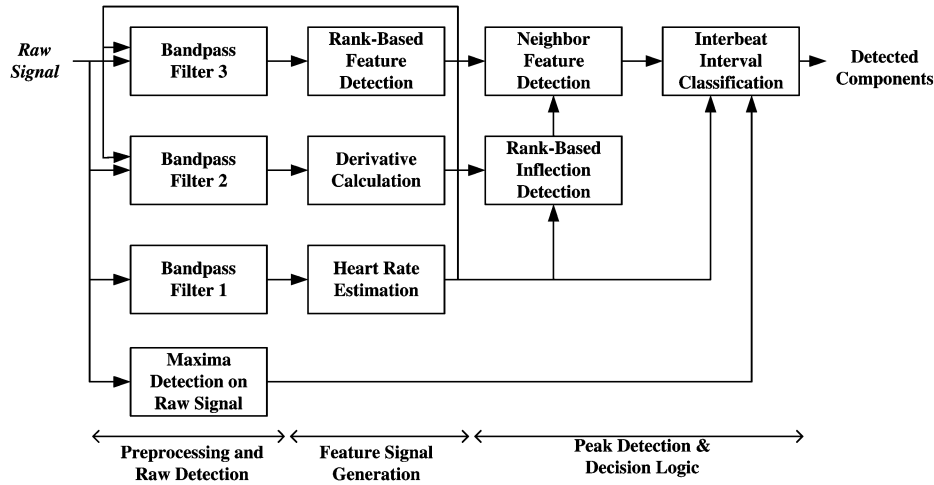


Fig. 4. Block diagram showing the architecture and individual stages of the new detection algorithm for peak component detection in pressure signals.

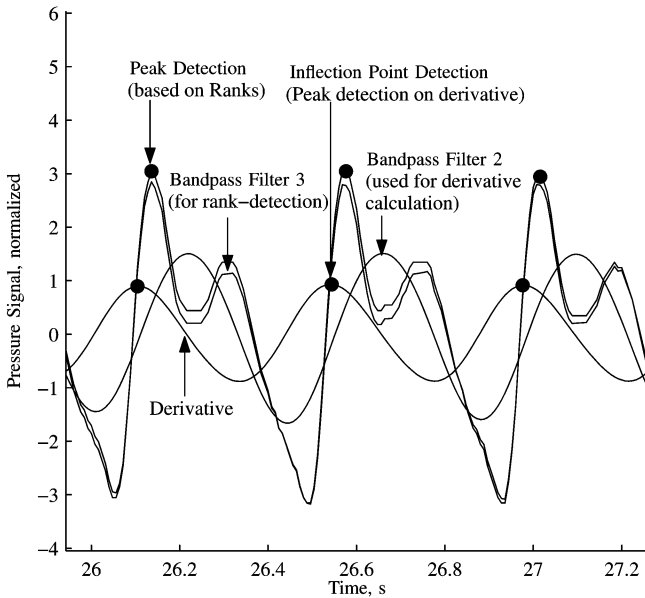


Fig. 5. Example illustrating the output of some of the stages performed by the detector during peak component detection in pressure signals.

relative amplitude and slope. Finally, the interbeat-interval stage uses this classification together with the estimated heart rate to make the final classification and detection of signal components. Since detection is made on the filtered signal, a second nearest neighbor algorithm finds the peaks in the raw signal that are closest to the detected components. Fig. 5 shows an example illustrating the output of some of the stages performed by the detector during peak component detection. Table I lists the pseudocode for this algorithm.

### B. Maxima Detection

Peak detection is performed at several stages in the algorithm. It is first used to detect all peaks in the raw signal prior to any preprocessing. Peak detection is also employed on each data partition of the filtered signal to find the relative amplitudes of the  $P_1$  component candidates and on the inflection points. The pseudocode for this function is shown in Table VI.

TABLE I  
ALGORITHM PSEUDOCODE

#### Algorithm $p = \text{PressureDetector}$

##### Inputs

$x := \text{Pressure signal.}$

$f_l := \text{Upper bound for the heart rate (optional).}$

$f_h := \text{Lower bound for the heart rate (optional).}$

##### Outputs

$p := \text{Detected peaks (samples).}$

##### Begin

$p_x := \text{DetectMaxima}(x, 0)$ . Locate maxima in  $x$ .

for  $j=1$  to  $\text{length}(x)$ , step size =  $w$ ,

$y_1 := \text{Bandpass filter } x: 0.5 f_l < f_p < 3 f_h$ .

$h := \text{EstimateHeartRate}(y_1)$ .

$y_2 := \text{Bandpass filter } x: 0.5 f_l < f_p < 2.5 \text{ median}(h)$ .

$y'_2 := \text{Estimate derivative of } y_2$ .

$p_2 := \text{DetectMaxima}(x, 90)$ . Peaks > 90th percentile.

$y_3 := \text{Bandpass filter } x: 0.5 f_l < f_p < 10 \text{ median}(h)$ .

$p_3 := \text{DetectMaxima}(x, 60)$ . Peaks > 60th percentile.

for  $k = 1$  to  $\text{length}(p_2)$ ,

$p_4 := \text{Find the closest } p_3 \text{ that follows } p_2$ .

end.

end.

$p := \text{IBICorrect}(p_4)$ . Correct FN and FP.

End.

### C. Preprocessing Stages

The preprocessing stage consists of three bandpass filters. The first filter removes the trend and eliminates high frequency noise. The resulting signal is used to estimate the heart rate which, in turn, is used to determine the cutoff frequency of the other two bandpass filters. The second filter further attenuates high frequency components and passes only frequencies that are less than 2.5 times the heart rate. The output of this filter only contains one cycle per heart contraction and eliminates enough high frequency power to ensure the signal derivative is not dominated by high frequency noise. The third bandpass filter detrends the signal by eliminating frequencies below half the minimum expected heart rate and slightly smoothes the signal

with an upper cutoff frequency equal to 10 times the estimated heart rate.

#### D. Spectral Heart Rate Estimation

In this stage, the pressure signal is partitioned and the power spectral density (PSD),  $\hat{p}(w)$ , of each segment is estimated. For the results reported here, we used the Blackman-Tukey method of spectral estimation. In general, any of the standard methods of spectral estimation could be used. The algorithm uses a harmonic PSD technique that combines  $n$  spectral components according to (1)

$$h(\omega) = \sum_{k=1}^n \min(\alpha \hat{p}(\omega), \hat{p}(k\omega)) \quad (1)$$

where  $\alpha$  ensures that the power of the harmonics added to  $h(\omega)$  does not exceed the power at the fundamental by more than a factor of  $\alpha$ . For our results we used  $\alpha = 2$  and  $n = 11$ . Table VII list the pseudocode for this function. The harmonic PSD technique combines the power of the fundamental and harmonic components. This technique has two main benefits: 1) it is less sensitive to signal morphology than traditional PSD estimates because it accounts for variations in the power distribution among harmonic frequencies, and 2) it achieves better frequency resolution of the lower harmonics by leveraging the relatively better resolution at the harmonic frequencies [26].

#### E. Peak Detection and Decision Logic

The detector uses nonlinear filters based on ranks for peak detection and decision logic. After preprocessing, a rank filter detects the peaks in each signal partition above the 60th percentile using a running window of 10 s. Since the signal has been detrended and smoothed, most of these peaks correspond to the  $P_1$  signal components. In the case of high-pressure ICP signals,  $P_2$  components are usually misclassified as  $P_1$  at this stage. Another rank filter applied to the derivative signal detects all maxima above the 90th percentile. These peaks correspond to the points of maximum slope, the signal inflection points.

This decision logic calculates the interbeat intervals of the detected candidate components. Whenever the detector has missed a component (false negative), the interbeat interval has an impulse which exceeds 1.75 the estimated heart rate. In the cases where the detector has over-detected a component (false positive), the impulse is “negative” showing an interbeat interval (IBI) less than 0.75 the estimated heart rate. Since missed and over-detected components create impulses in the interbeat series, this stage uses median-based filters to remove this impulsive noise. These detection errors can be easily located by applying a simple set of thresholds to the residual signal, i.e., the difference between the IBI series and the filter output.

#### F. Nearest Neighbor Decision Logic

This stage combines slope and beat amplitude information to decide whether a peak in the smoothed signal is a valid  $P_1$ . These two metrics are combined by using a simple nearest neighbor algorithm. The inputs to this stage are two arrays containing the time location of inflection points (slope maxima), and the candidate peak components obtained using the rank filter. The nearest neighbor algorithm locates each candidate component that immediately follows each inflection point. This selects the peaks that meet the relative amplitude requirement and that are immediately preceded by a large slope, which

eliminates  $P_2$  components with higher amplitude than  $P_1$  in high-pressure waves. In the case of low-frequency waves,  $P_1$  has usually the highest amplitude component, but the amplitude of  $P_3$  components may be above the 60th percentile threshold. These are also eliminated in this stage.

#### G. IBI Classification Logic

After the candidate peaks have passed the relative amplitude and slope criteria in the previous stage, the final classification is performed based on the interbeat-intervals (IBI) of the time series containing the candidate peaks. Assuming subjects do not have significant arrhythmias, the number of false positives and false negatives can be reduced by imposing time constraints on the IBI series. As mentioned earlier, whenever the detector has missed a peak, the interbeat interval has an impulse which exceeds twice the estimated heart rate. In the cases where the detector has over-detected, the impulse is in the opposite direction and is less than half the estimated heart rate.

This stage calculates the first difference,  $x(n) - x(n - 1)$ , of the peak-to-peak interval series. It then searches the time series for instances where the interbeat distance is less than 0.75 the median IBI. This is considered an over-detection, and  $x(n)$  is removed from the candidate time series. This stage then searches for cases where the IBI is greater than 1.75 the median IBI, which are considered missed peaks. To correct this the algorithm searches the initial maxima time series, obtained before preprocessing and adds the component that minimizes the interbeat variability. This process is repeated until all the candidate components fall within the expected range or the maximum number of allowed corrections is reached.

Finally, two rank-order filters at the 90th and 10th percentile are applied to the IBI series in order to detect the locations of possible misdetections and over detections that were within the accepted heart rate limits.

### III. METHODS

#### A. Validation Database and Manual Annotation

Several standard databases are available for the evaluation of QRS detection algorithms. These include the MIT-BIH, AHA, and CSE databases [27]. Presently, there are no benchmark databases available to assess the performance of pressure detection algorithms on ICP, ABP, or POX. There are two free databases of blood pressure waveforms: Physionet and Eurobavar but neither of these has manually annotated pressure components.

We assessed the performance of our algorithm on ICP, ABP, and SpO<sub>2</sub> signals acquired from the Pediatric Intensive Care Unit (PICU) at Doernbecher Children’s Hospital, Oregon Health & Science University. The signals were acquired by a data acquisition system in the Complex Systems Laboratory (CSL) and are part of the CSL database. The patient population for this study was limited to subjects admitted for traumatic brain injury, sepsis, and cardiac conditions. The sampling rate was 125 Hz and the resolution was  $\pm 0.2$  mmHg (8 bits, 256 levels). Although this sampling rate is not sufficient for some types of cardiac arrhythmia analysis, it is adequate for pressure pulse contour analysis and the other applications listed earlier. A total of 42 539 beats were selected using a random number generator from a population of 210 patients (60 TBI, 60 Sepsis, and 90 cardiac). Two patients from each group were randomly selected. A 60 minute record was then randomly chosen from the entire recording available for each patient.

TABLE II

SENSITIVITY AND POSITIVE PREDICTIVITY OF THE DETECTION ALGORITHM FOR ICP, ABP, AND ECG SIGNALS. THE TABLE SHOWS THE  $Se$  AND  $+P$  RESULTS FOR ACCEPTANCE INTERVALS OF 8.0, 16.0, 24.0, AND 48 MS. THESE RESULTS USED THE EXPERT MANUAL ANNOTATIONS (DT) ON 42 539 BEATS RANDOMLY SELECTED FROM A PEDIATRIC INTENSIVE CARE UNIT PATIENT POPULATION. THE SEGMENTS INCLUDED REGIONS OF SEVERE ARTIFACT

Interval(ms)	8.0	16.0	24.0	48.0
ICP $Se$	90.62	98.23	99.17	99.30
ICP $+P$	89.14	96.55	97.47	97.60
ABP $Se$	99.32	99.51	99.52	99.53
ABP $+P$	99.14	99.33	99.34	99.34
SpO <sub>2</sub> $Se$	83.26	96.45	98.85	99.27
SpO <sub>2</sub> $+P$	82.36	95.54	97.93	98.35

TABLE III

ALGORITHM'S SENSITIVITY AND POSITIVE PREDICTIVITY VALIDATED AGAINST TWO EXPERTS MANUAL ANNOTATIONS OF 2300 BEATS OF RANDOMLY SELECTED ICP SIGNALS FOR ACCEPTANCE INTERVALS (AI) OF 16.0 AND 24.0 MS. THE TABLE SHOWS THE ALGORITHM'S PERFORMANCE (AD) AGAINST THE TWO EXPERTS (DT AND JM), AND THE CONSISTENCY OF THE EXPERTS BETWEEN THEMSELVES

ICP	AI	$Se$	$+P$	FN	FP
AD-DT	16.0	99.45	99.45	12	12
AD-JM	16.0	99.35	99.35	15	15
DT-JM	16.0	99.57	100.0	10	0
AD-DT	24.0	98.84	98.84	27	3
AD-JM	24.0	99.35	99.35	15	15
DT-JM	24.0	100.0	100.0	0	0

One expert performed manual annotations for all the six records. Each record was divided into nonoverlapping segments of 1 minute duration. The expert visually classified each segment as "normal", "corrupted", or "absent." A "normal" segment was defined as a segment in which the noise corrupting the signal was not "abnormal," in the sense that the corrupting noise is typically present for the specific waveform in a critical care environment. Examples of this type of noise are baseline drift, amplitude modulation with respiration, power-line interference, and morphology changes. A "corrupted" segment was defined as a segment in which the signal contains substantial artifact that prevents standard analysis methods from being effective. Examples include device saturation (clipping) and external perturbation of the sensor (catheter movement by nurse of patient). Segments in which the signal was lost (constant) for more than 10 s were classified as "absent." Instructions for classifying segments and examples are available in [28].

Once the segments were classified, the expert manually labeled every beat in all six records (42,539 beats). A second expert manually annotated 7128 beats of the normal and corrupted segments.

### B. Benchmark Parameters

Following the guidelines proposed by the Association for the Advancement of Medical Instrumentation (AAMI), two benchmark parameters were used to assess the algorithms performance: sensitivity and positive predictivity [29]. Sensitivity and positive predictivity are defined as

$$Se = \frac{TP}{TP + FN} \quad (2)$$

$$+P = \frac{TP}{TP + FP} \quad (3)$$

where  $TP$  is the number of true positives,  $FN$  the number of false negatives, and  $FP$  the number of false positives. The

TABLE IV

ALGORITHM'S SENSITIVITY AND POSITIVE PREDICTIVITY VALIDATED AGAINST TWO EXPERTS MANUAL ANNOTATIONS OF 2179 BEATS OF RANDOMLY SELECTED ABP SIGNALS FOR ACCEPTANCE INTERVALS (AI) OF 16.0 AND 24.0 MS. THE TABLE SHOWS THE ALGORITHM'S PERFORMANCE (AD) AGAINST THE TWO EXPERTS (DT AND JM), AND THE CONSISTENCY OF THE EXPERTS BETWEEN THEMSELVES

ABP	AI	$Se$	$+P$	FN	FP
AD-DT	16.0	100.0	100.0	0	0
AD-JM	16.0	100.0	100.0	0	0
DT-JM	16.0	100.0	100.0	0	0
AD-DT	24.0	100.0	100.0	0	0
AD-JM	24.0	100.0	100.0	0	0
DT-JM	24.0	100.0	100.0	0	0

TABLE V

ALGORITHM'S SENSITIVITY AND POSITIVE PREDICTIVITY VALIDATED AGAINST TWO EXPERTS MANUAL ANNOTATIONS OF 2649 BEATS OF RANDOMLY SELECTED SpO<sub>2</sub> SIGNALS FOR ACCEPTANCE INTERVALS (AI) OF 16.0 AND 24.0 MS. THE TABLE SHOWS THE ALGORITHM'S PERFORMANCE (AD) AGAINST THE TWO EXPERTS (DT AND JM), AND THE CONSISTENCY OF THE EXPERTS BETWEEN THEMSELVES

SpO <sub>2</sub>	AI	$Se$	$+P$	FN	FP
AD-DT	16.0	99.97	99.59	1	10
AD-JM	16.0	99.87	99.68	3	8
DT-JM	16.0	99.81	100.0	5	0
AD-DT	24.0	99.97	99.59	1	10
AD-JM	24.0	99.94	99.75	1	6
DT-JM	24.0	100.0	100.0	0	0

sensitivity  $Se$  indicates the percentage of true beats that were correctly detected by the algorithm. The  $+P$  indicates the percentage of beat detections which were labeled as such by the expert.

### C. Algorithm Assessment

The algorithm was validated prospectively against expert annotated detections generated by two different experts on ICP, ABP, and SpO<sub>2</sub> signals. The performance of the algorithm was first assessed on the randomly chosen segments without taking into consideration whether they contained portions of significant artifact. After an expert manually classified each minute as normal, corrupted, or absent, the algorithm performance was assessed using each experts' manual annotations as the "true" peaks on the normal and corrupted segments. The algorithm was developed using pressure signals from different patients than those used for performance assessment. The assessment was measured only once without any parameter tuning.

## IV. RESULTS

Table II reports the algorithm's sensitivity and positive predictivity for the different pressure signals and acceptance intervals of 8.0, 16.0, 24.0, and 48.0 ms. These are based on one expert's manual annotations for all 42 539 beats including segments classified as normal, corrupted, and absent. Tables III–V report the algorithm's sensitivity and positive predictivity on ICP, ABP, and SpO<sub>2</sub> signals, respectively. These tables show the algorithm's performance (AD) compared with two different experts (DT & JM) on segments classified as normal or corrupted. The inter-expert agreement is also reported with DT used as the "true" peaks. The algorithm's average sensitivity on the 42 539 beats is 99.36%,  $(99.30 + 99.53 + 99.27)/3$ ; with a 98.43%

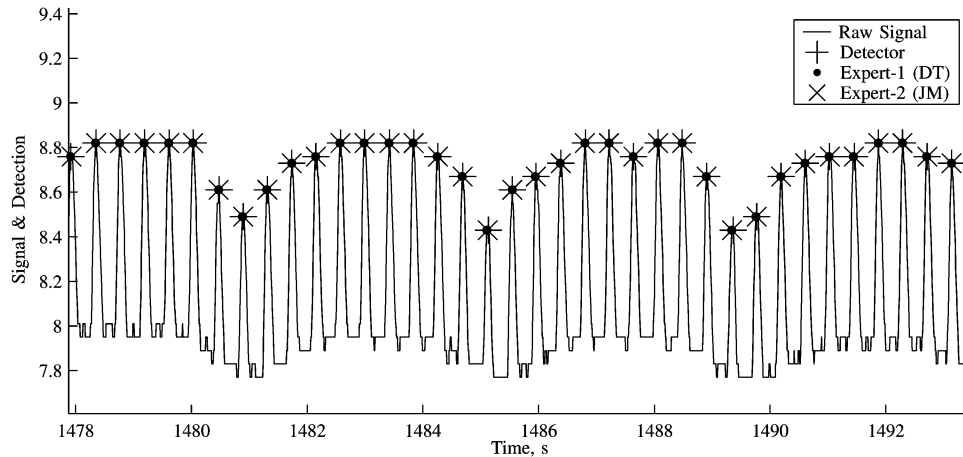


Fig. 6. Illustrative example showing an ICP signal and the percussion peaks ( $P_1$ ) identified by the two experts and the detection algorithm. In this case both experts and the algorithm were in perfect agreement.

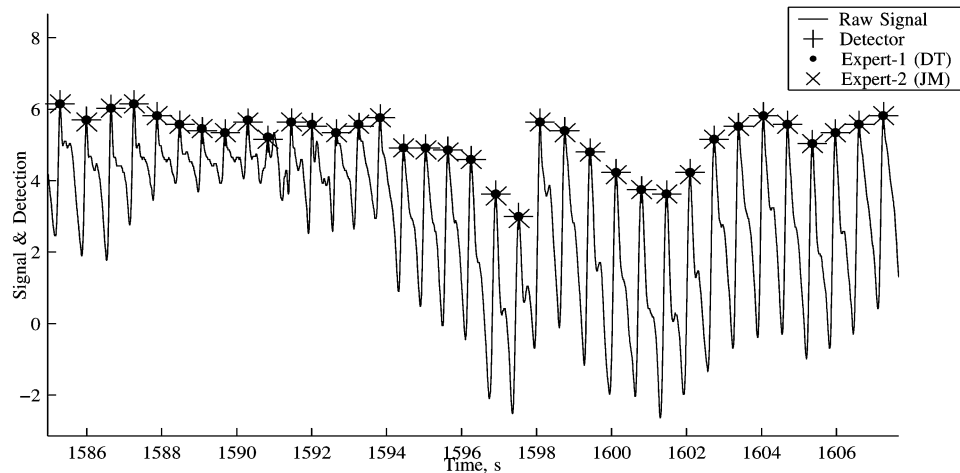


Fig. 7. Illustrative example showing an ICP signal and the percussion peaks ( $P_1$ ) identified by the two experts and the detection algorithm. Again both experts and the algorithm were in perfect agreement despite the changing morphology and the different character than the signal shown in Fig. 6.

$(99.60 + 99.34 + 99.35)/3$ , positive predictivity for an acceptance interval of 16 ms ( $\pm 2$  samples).

## V. DISCUSSION

### A. Results

The results show that the algorithm is nearly as accurate as the experts are with one-another. Figs. 6 and 7 show examples of ICP percussion peaks. Note that the signal morphology in Fig. 7 is considerably different from Fig. 6. Fig. 8 shows some examples when the algorithm detected different peaks than the experts in a  $\text{SpO}_2$  signal. Note that this segment is corrupted by clipping artifact and the algorithm continued to identify peaks (over detection). When clipping occurs, the algorithm tries to interpolate and perform component detection trying to minimize the interbeat interval variability. Experts did not try to interpolate in segments where the signal was absent due to device saturation. This reduces the algorithm's reported sensitivity and positive predictivity. Fig. 8 also shows a missed peak after the clipped region. In general, regions where artifact occurs have a slight effect on normal beats that are close. This occurs because the artifacts can affect the rank-filters' baseline and, therefore, the estimated relative amplitude and estimated slope.

Since data was sampled at 125 Hz and there were several regions with clipping, we chose an acceptance interval of 16 ms ( $\pm 2$  samples). We expect that similar or better performance would be obtained on signals sampled at a higher rate.

### B. Algorithm Limitations and Computational Efficiency

Most stages are computationally efficient enough to implement in a nearly real-time block processing architecture. However, the IBI-based decision logic stage eliminates all the candidate components which do not meet timing requirements and adds components that minimize the IBI variability. This stage is computationally inefficient because it requires several searching and sorting operations. This is exacerbated by the repeated passes through this step until no further corrections are made. If the number of allowed corrections is not limited, the algorithm may continue this indefinitely. For the results reported here we limited the number of corrections to 5 times the initial number of false detections.

### C. Validation Databases

Although there are several standard databases available for the evaluation of QRS detection algorithms, there are no benchmark databases presently available to assess the performance of

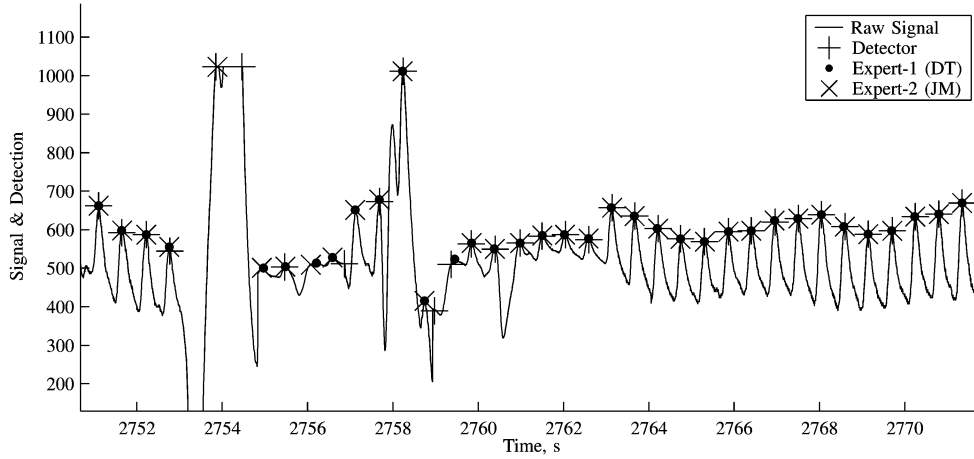


Fig. 8. Example showing a SpO<sub>2</sub> signal and the systolic peak (SBP) identified by the two experts and the detection algorithm. In this case the experts and algorithm labeled different peaks in the regions of artifact. Clearly Expert-1 (DT) made the correct choice and Expert-2 (JM) needs more training.

TABLE VI  
FUNCTION PSEUDOCODE: DETECTMAXIMA

---

Function  $p = \text{DetectMaxima}$   
**Inputs**  
 $x :=$  Input signal.  
 $t_r :=$  Percentile threshold.  
**Outputs**  
 $m :=$  Detected peaks above  $t_r$ (samples).  
**Begin**  
 $l_d :=$  Number of Samples of  $x$ .  
 $m :=$  Find the indexes of  $x$  such that:  $x_{k-1} \leq x_k \geq x_{k+1}$   
 $m_t :=$  Find  $x(m)$  such that  $x(m) \geq t_r$  percentile.  
**End.**

---

TABLE VII  
FUNCTION PSEUDOCODE: ESTIMATEHEARTRATE

---

Function  $p = \text{EstimateHeartRate}$   
**Inputs**  
 $x :=$  Input signal.  
 $w :=$  Window length (samples).  
**Outputs**  
 $h :=$  Estimated heart rate (1 estimate per  $w$ ).  
**Begin**  
Initialize array  $h_r$ .  
for  $k = 1$  to  $\text{length}(x)$ , step size  $w$ ,  
if  $(k + w < \text{length}(x) - w - 1)$ ,  
 $x_s := x(k \text{ to } k + w - 1)$ .  
 $[p, f] :=$  Estimate PSD in  $x_s$  (Blackman-Tukey).  
 $[p_h, f_h] :=$  HarmonicPSD(p,f).  
 $m :=$  Find the frequency where the PSD is maximum.  
 $h_r :=$  Add the heart rate estimate to the  $hr$  array.  
else  
 $x_s := x(k \text{ to } \text{length}(x))$ .  
 $[p, f] :=$  Estimate PSD in  $x_s$  (Blackman-Tukey).  
 $[p_h, f_h] :=$  HarmonicPSD(p,f).  
 $m :=$  Find the frequency where the PSD is maximum.  
 $h_r :=$  Add the heart rate estimate to the  $hr$  array.  
end.  
**End.**

---

pressure detection algorithms. Validation databases with manually annotated beats by human experts are needed in order to provide reproducible and comparable performance assessment of pressure detection algorithms.

Our validation dataset is publicly available at <http://bsp.pdx.edu> to provide other developers annotated examples that can be used to validate their beat detection algorithms. Nonetheless, we caution developers and users about the risk of validation databases. If developers use these datasets for development, the performance is favorably biased by the tuning and algorithm design that occurs during development. These algorithms may have worse performance when applied prospectively to new datasets. Although validation databases contain large number of annotated peaks, detection algorithms can still be favorably tuned to the common cardiac physiology of the patient population, which is often a narrow subgroup that has been targeted for their common pathologies. Ideally, validation should be performed prospectively by a third party on data that is unavailable to developers. Some progress toward this higher standard of performance has been achieved through the Computers and Cardiology challenges. Independent third-party validation of algorithms on proprietary data with standardized performance measures would significantly advance the quality of detection algorithms as a whole.

## VI. CONCLUSION

We described a new automatic beat detection algorithm that can be used to detect the percussion component in ICP signals and the systolic peak in ABP and SpO<sub>2</sub> signals. Although there is a substantial body of literature describing QRS detection algorithms, there are almost no published descriptions or assessments of pressure detection algorithms. These algorithms are needed for many applications and research.

Our algorithm consists of several stages. It relies on the estimated heart rate to choose the cutoff frequencies used by the pre-processing bandpass filters and to aid the discrimination of false negatives and false positives on the interbeat-interval decision logic stage. It uses three bandpass filters to eliminate drift and attenuate high frequency noise. It uses nonlinear rank order filters for peak detection and decision logic. The algorithm was validated prospectively (validation dataset was not available during algorithm development). The algorithm was run only once on the dataset and achieved a sensitivity of 99.36% and a positive

TABLE VIII  
FUNCTION PSEUDOCODE: IBICORRECT

---

Function  $p = \text{IBICorrect}$

Inputs

$p :=$  Location of detected peaks.

$m :=$  All the peaks in the signal before preprocessing.

$h_r :=$  Heart rate estimate using PSD.

Outputs

$p_c :=$  Detected peaks after IBI correction.

Begin

Nearest neighbor and IBI based corrections:

Correct peaks' location error due to preprocessing.

for  $k=1$  to  $\text{length}(p)$ ,

$p_c :=$  Find  $m$  closest to  $p$ .

end.

Correct False Negatives (FN) and False Positives(FP)

$d :=$  Interbeat intervals:  $p_{n+1} - p_n$ .

$f_n :=$  Find indexes of  $d$  where  $d > 1.75 h_r$ .

$e_f :=$  Estimated number of peaks based on  $h_r$ .

while  $f_n \neq 0$  and  $\text{count} > e_f$ ,

    for  $k = 1$  to  $\text{length}(f_n)$ .

$x_s :=$  Signal segment from  $m(k)$  to  $p(m(k) + 1)$ .

$p_c :=$  Perform FN correction on signal segment.

    end.

Correct False Positives (FP).

$d :=$  Interbeat intervals:  $p_{n+1} - p_n$ .

$f_p :=$  Find indexes of  $d$  where  $d < 0.75 h_r$ .

for  $k = 1$  to  $\text{length}(f_p)$ .

$p_c :=$  Take the FP out of the  $p_c$  array.

end.

$d :=$  Interbeat intervals after correction.

$y_{90} :=$  Filter  $d$  using Rank filter:  $t_r = 90^{\text{th}}$ .

$y_{10} :=$  Filter  $d$  using Rank filter:  $t_r = 10^{\text{th}}$ .

$f_n :=$  Find indexes of  $d$  where  $d > y_{90}$ .

$f_p :=$  Find indexes of  $d$  where  $d < y_{10}$ .

$p_c :=$  Run detector around  $f_n$  and  $f_p$  and correct.

if (number of  $p_c$  equals  $e_f$ ) or ( $\text{count} > \text{maxcount}$ ).

    stop correction.

end.

end.

End.

---

predictivity of 99.43% when compared with expert manual annotations of ICP, ABP, and SpO<sub>2</sub> signals from the CSL Database (OHSU).

We also described a validation dataset and the CSL Database of the Doernbecher Children's Hospital (Oregon Health & Science University). This validation dataset is publicly available as a standard database for algorithm validation.

APPENDIX

The following Tables provide the pseudocode of the functions used by pressure detector algorithm.

ACKNOWLEDGMENT

The authors wish to acknowledge the support of the Northwest Health Foundation and the Doernbecher Children's Hospital Foundation.

REFERENCES

- [1] B.-U. Köhler, C. Henning, and R. Orglmeister, "The principles of software QRS detection," *IEEE Eng. Med. Biol. Mag.*, vol. 21, no. 1, pp. 42–57, Jan.-Feb. 2002.
- [2] L. Anonelli, W. Ohley, and R. Khamlach, "Dicrotic notch detection using wavelet transform analysis," in *Proc. 16th Annu. Int. Conf. IEEE Engineering in Medicine and Biology Society*, vol. 2, 1994, pp. 1216–1217.
- [3] P. F. Kinias and M. Norusis, "A real time pressure algorithm," *Comput. Biol. Med.*, vol. 11, pp. 211–211, 1981.
- [4] M. Aboy, J. McNames, and B. Goldstein, "Automatic detection algorithm of intracranial pressure waveform components," in *Proc. 23th Int. Conf. IEEE Engineering in Medicine and Biology Society*, vol. 3, 2001, pp. 2231–2234.
- [5] M. Aboy, C. Crespo, J. McNames, and B. Goldstein, "Automatic detection algorithm for physiologic pressure signal components," in *Proc. 24th Int. Conf. IEEE Engineering in Medicine and Biology Society and Biomedical Engineering Society*, vol. 1, 2002, pp. 196–197.
- [6] E. G. Caiani, M. Turiel, S. Muzzupappa, A. Porta, G. Baselli, S. Cerutti, and A. Malliani, "Evaluation of respiratory influences on left ventricular function parameters extracted from echocardiographic acoustic quantification," *Physiol. Meas.*, vol. 21, pp. 175–186, 2000.
- [7] J. D. Doyle and P. W. S. Mark, "Analysis of intracranial pressure," *J. Clin. Monitoring*, vol. 8, no. 1, pp. 81–90, 1992.
- [8] G. Parati, M. Di Rienzo, and G. Mancia, "How to measure baroreflex sensitivity: From the cardiovascular laboratory to daily life," *J. Hypertension*, vol. 18, pp. 7–19, 2000.
- [9] M. Di Rienzo, P. Castiglioni, G. Mancia, A. Pedotti, and G. Parati, "Advances in estimating baroreflex function," *IEEE Eng. Med. Biol. Mag.*, vol. 20, no. 2, pp. 25–32, Mar./Apr. 2001.
- [10] M. Di Rienzo, G. Parati, P. Castiglioni, R. Tordi, G. Mancia, and A. Pedotti, "Baroreflex effectiveness index: An additional measure of baroreflex control of heart rate in daily life," *Am. J. Physiol. Regulatory, Integrative, Comparative Physiol.*, vol. 280, pp. R744–R751, 2001.
- [11] E. G. Caiani, M. Turiel, S. Muzzupappa, A. Porta, L. P. Colombo, and G. Baselli, "Noninvasive quantification of respiratory modulation on left ventricular size and stroke volum," *Physiol. Meas.*, vol. 23, pp. 567–580, 2002.
- [12] G. E. McVeigh, C. W. Bratteli, C. M. Alinder, S. Glasser, S. M. Finkelstein, and J. N. Cohn, "Age-related abnormalities in arterial compliance identified by pressure contour analysis," *Hypertension*, vol. 33, pp. 1392–1398, 1999.
- [13] W. Holsinger, K. Kempner, and M. Miller, "A QRS preprocessor based on digital differentiation," *IEEE Trans. Biomed. Eng.*, vol. BME-18, pp. 121–127, 1971.
- [14] M.-E. Nygard and J. Hulting, "An automated system for (ecg) monitoring," *Comput. Biomed. Res.*, vol. 12, pp. 181–202, 1979.
- [15] M. Okada, "A digital filter for the QRS complex detection," *IEEE Trans. Biomed. Eng.*, vol. BME-26, pp. 700–703, 1979.
- [16] J. Fraden and M. Neumann, "QRS wave detection," *Med. Biol. Eng. Comput.*, vol. 18, pp. 125–132, 1980.
- [17] J. Pan and W. Tompkins, "A real-time QRS detection algorithm," *IEEE Trans. Biomed. Eng.*, vol. BME-32, pp. 230–236, 1985.
- [18] G. Friesen, T. Jannett, M. Jadallah, S. Yates, S. Quint, and H. Nagle, "A comparison of the noise sensitivity of nine QRS detection algorithms," *IEEE Trans. Biomed. Eng.*, vol. 37, no. 1, pp. 85–98, Jan. 1990.
- [19] F. Gritzali, "Toward a generalized scheme for QRS detection in ECG waveforms," *Signal Process.*, vol. 15, pp. 183–192, 1988.
- [20] P. Hamilton and W. Tompkins, "Quantitative investigation of QRS detection rules using the (mit/bih) arrhythmic database," *IEEE Trans. Biomed. Eng.*, vol. BME-33, pp. 1157–1165, 1986.
- [21] —, "Adaptive matched filtering for QRS detection," in *Proc. Annu. Int. Conf. IEEE Engineering in Medicine and Biology Society*, 1988, pp. 147–148.
- [22] V. Afonso, W. Tompkins, T. Nguyen, and S. Luo, "ECG beat detection using filter banks," *IEEE Trans. Biomed. Eng.*, vol. 46, no. 2, pp. 192–202, Feb. 1999.



- [23] S. Kadambe, R. Murray, and G. Boudreaux-Bartels, "Wavelet transform-based QRS complex detector," *IEEE Trans. Biomed. Eng.*, vol. 46, no. 7, pp. 838–848, Jul. 1999.
- [24] W. W. Nichols and M. F. O'Rourke, *McDonald's Blood Flow in Arteries: Theoretical, Experimental and Clinical Principles*, 4th ed. London, U.K.: Arnold, 1998.
- [25] B. North, "Intracranial pressure monitoring," in *Head Injury*, P. Reilly and R. Bullock, Eds. London, U.K.: Chapman & Hall, 1997, pp. 209–216.
- [26] M. H. Hayes, *Statistical Digital Signal Processing and Modeling*. New York: Wiley, 1996.
- [27] MIT-BIH ECE Database. Massachusetts Inst. Technol., Cambridge. [Online]. Available: <http://ecg.mit.edu>
- [28] M. Aboy. (2002) Instructions for Labeling Segments Used on the Evaluation of the BSP-Automatic Pressure Detection Algorithm. Portland State University. [Online]. Available: <http://bsp.pdx.edu>
- [29] (1998) ANSI/AAMI CE57: Testing and Reporting Performance Results of Cardiac Rhythm and ST Segment Measurement Algorithms. (AAMI Recommended Practice/American National Standard. [Online]. Available: <http://www.aami.org>



**Mateo Aboy** (M'98) received the double B.S. degree (*magna cum laude*) in electrical engineering and physics from Portland State University (PSU), Portland, OR, in 2002. In 2004, he received the M.S. degree (*summa cum laude*) in electrical and computer engineering from PSU and the M.Phil (DEA) degree from the University of Vigo (ETSIT-Vigo), Vigo, Spain, where he is working towards the Ph.D. degree in the Signal Theory and Communications Department.

Since September 2000, he have been a research member of the Biomedical Signal Processing Laboratory (PSU). He has been with the Electronics Engineering Technology Department at Oregon Institute of Technology, Portland, since 2005. His primary research interest is statistical signal processing.

Mr. Aboy is a lifetime honorary member of the Golden-Key Honor Society, a past Chapter President of HKN (International Electrical Engineering Honor Society), and past Corresponding Secretary of TBP (National Engineering Honor Society).



**James McNames** (M'99–SM'03) received the B.S. degree in electrical engineering from California Polytechnic State University, San Luis Obispo, in 1992. He received M.S. and Ph.D. degrees in electrical engineering from Stanford University, Stanford, CA, in 1995 and 1999, respectively.

He has been with the Electrical and Computer Engineering Department at Portland State University, Portland, OR since 1999, where he is currently an Associate Professor. He has published over 90 journal and conference papers. His primary research interest is statistical signal processing with biomedical applications.

He founded the Biomedical Signal Processing (BSP) Laboratory ([bsp.pdx.edu](http://bsp.pdx.edu)) in fall 2000. The mission of the BSP Laboratory is to advance the art and science of extracting clinically significant information from physiologic signals. Members of the BSP Laboratory primarily focus on clinical projects in which the extracted information can help physicians make better critical decisions and improve patient outcome.



**Tran Thong** (S'70–M'76–SM'82–F'89) received the B.S.E.E. degree from Illinois Institute of Technology, Chicago, in 1972, and the M.S.E. and M.A. (EE) degrees in 1973 and 1974 and the Ph.D. degree in electrical engineering in 1975 from Princeton University, Princeton, NJ.

He worked at Bell Laboratories, Litton Industries, General Electric Company, Tektronix Inc. From 1993 to 2001, he was the Engineering Vice-President of Micro Systems Engineering, Inc., a Biotronik company, where he was responsible for the development of pacemakers and implantable defibrillators. Since 1990, he has been an Adjunct Professor of Electrical and Computer Engineering in the OGI School of Science & Engineering, Oregon Health & Science University, Beaverton. In 2002, he joined the Department of Biomedical Engineering of the OGI School of Science and Engineering as an Assistant Professor. He has published over 50 articles and conference papers, and holds 23 U.S. patents. His current research is directed toward cardiac rhythm management and biomedical signal processing.

Dr. Thong is a member of Sigma Xi, Tau Beta Pi, and Eta Kappa Nu.

**Daniel Tsunami**, photograph and biography not available at the time of publication.



**Miles S. Ellenby** received the B.E. and M.E. degrees degree (1986) and masters (1987) degrees in electrical engineering from the University of Illinois, Urbana-Champaign, in 1986 and 1987, respectively. He received the M.D. degree from the University of Chicago in 1990.

He did his Pediatrics residency (1991–1994) at the Children's Hospital of Philadelphia, followed by a year as chief resident (1994–1995). He did a fellowship in Pediatric Critical Care Medicine in the combined University of California/San Francisco

Children's Hospital of Oakland program (1995–1998). He joined the faculty at Oregon Health & Science University in 2000, where he is now an Assistant Professor of Pediatrics. He specializes in critical care medicine with a special interest in the care of children with congenital heart disease. His research interests are in cardiovascular monitoring, complex systems analysis and biological signals processing.



**Brahm Goldstein** (A'99) received the B.S. degree in biological science from Northwestern University, Evanston, IL, in 1977 and the M.D. degree from the State University of New York (SUNY) Upstate Medical Center at Syracuse in 1981. His clinical training included residency in pediatrics at the University of California at Los Angeles (UCLA) Medical Center and fellowships in pediatric cardiology and pediatric critical care medicine at Children's Hospital and Massachusetts General Hospital, Boston, respectively.

After serving as a faculty member at the Harvard Medical School, Cambridge, MA, and at the University of Rochester School of Medicine and Dentistry, Rochester, MN, he joined the Oregon Health & Science University, Portland, where he now is Professor of Pediatrics and Director of the Pediatric Clinical Research Office. His research interests include the study of heart rate variability and the acquisition and analysis of biomedical signals in critical illness and injury (brain injury and septic shock in particular). He formed the Complex Systems Laboratory ([www.ohsuhealth/dch/complex](http://www.ohsuhealth/dch/complex)) in 1998 to study complex disease states in critically ill and injured children.

Dr. Goldstein is a diplomate of the American Board of Pediatrics and its sub-board pediatric critical care medicine.